Front. Earth Sci. 2024, 18(4): 743−751
https://doi.org/10.1007/s11707-024-1115-0

RESEARCH ARTICLE

Experimental analysis of dust deposition and physical weathering intensity in the Gobi Desert

Xunming WANG[1,2], Danfeng LI (✉)[1], Bingqi ZHU[1], Zhenting WANG[3], Caixia ZHANG[3], Xin GENG[1], Likun HAN[1], Yang ZHENG[1], Diwen CAI[1]

1 Key Laboratory of Water Cycle and Related Land Surface Processes, Institute of Geographic Sciences and Natural Resources Research, Chinese Academy of Sciences, Beijing 100101, China
2 College of Resources and Environment, University of Chinese Academy of Sciences, Beijing 100049, China
3 Key Laboratory of Desert and Desertification, Northwest Institute of Eco-Environment and Resources, Chinese Academy of Sciences, Lanzhou 730000, China

Abstract Surface soil materials from the Gobi Desert were sieved into fraction groups of 0.063–0.125, 0.125–0.25, 0.25–0.5, 0.5–1, and 1–2 mm. These samples were placed in a field for a physical weathering and dust deposition experiment. In the natural Gobi Desert environment, the dust-sized fractions (< 0.063 mm in diameter) produced by physical weathering and via dust deposition in the above groups were 1387 ± 124, 702 ± 70, 698 ± 47, 742 ± 101, and 769 ± 75 $g \cdot m^{-2}$, respectively, from 18 October 2020 to 18 December 2021. Dust deposition during the same period was 611 ± 55 $g \cdot m^{-2}$. For the same respective groups, 5.32 ± 0.76%, 0.58 ± 0.27%, 0.53 ± 0.18%, 0.80 ± 0.52%, and 0.98 ± 0.31% (by weight) of the bulk samples were weathered into dust-sized fractions during the experimental period. The physical weathering intensities were 23.95%, 14.96%, 8.90%, and 2.81% by weight for fraction groups of 2–4, 4–8, 8–16, and > 16 mm, respectively. The fine-grained materials of the gravel were more sensitive to physical weathering than coarse materials. In natural environments, the processes of dust deposition and physical weathering were key factors affecting the surface topographical equilibrium of the Gobi Desert and dust emission in Asia.

Keywords physical weathering, dust deposition, Gobi Desert, sand activity

1 Introduction

The Gobi Desert (also referred to as gravel desert or rocky desert) is located in Central Asia and has an area of 1.3×10^6 km^2. The desert surface is covered by a layer of gravel or coarse materials and the underlying surfaces are filled with sand, silt, or clay (Cooke, 1970; Pelletier et al., 2007). Previous studies (Vassallo et al., 2005; Heumann et al., 2018; Lu et al., 2019; Yu et al., 2019) have suggested that the Gobi Desert was developed since the Pliocene. At least from two thousand years ago to the present, there were similar landscapes, as recorded in ancient Chinese literature (e.g., Ban et al., 1962). The surface processes that have occurred in the Gobi Desert mainly include aeolian, hydrological, weathering, dust deposition, etc. (e.g., Wang et al., 2008; Liu et al., 2022) (Fig. 1). Gravel on the Gobi Desert surface may have developed under short-term rapid accumulation (Hülle, et al., 2010; Lehmkuhl et al., 2018). Soil below the Gobi Desert surface shows an abundance of dust-sized particles (fractions < 0.063 mm in diameter), and gravel and consolidation characteristics may protect these dust-sized particles from wind erosion (Wang et al., 2012b; Mu et al., 2018). Only the erodible dust-sized fractions produced by surface processes (e.g., Zobeck, 1991) could be re-emitted as the major sources for dust emissions (Wang et al., 2004; Wang et al., 2008; Wang et al., 2019; Filonchyk, 2022). However, under conditions that do not produce erodible dust-sized fractions, the Gobi Desert could not be the potential source area of Asian dust storms, and the surface equilibrium could not be maintained over thousands of years.

Annual precipitation in the Gobi Desert is usually less than 100 mm (Wang et al., 2008). Consequently, there have been very few modern fluvial activities occurring on the Gobi Desert, and therefore, only two major mechanisms for replenishing dust-sized fractions on Gobi Desert surfaces exist. One mechanism for producing dust-sized fractions is weathering (e.g., Ollier, 1969; Camuffo,

Received May 22, 2023; accepted December 21, 2023

E-mail: lidf@igsnrr.ac.cn

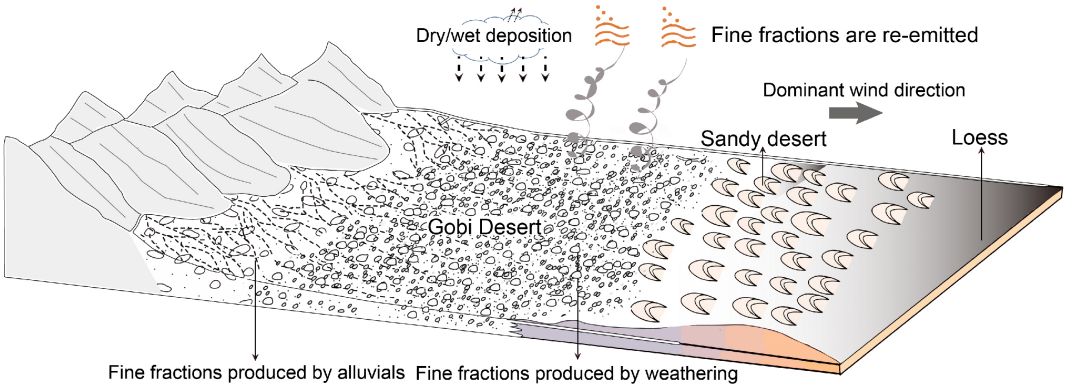

Fig. 1 Schematic diagram of Gobi Desert surface processes.

1995; McFadden et al., 2005; Liu et al., 2007; Eppes et al., 2010; Dorn, 2011; Buckman, et al., 2021), and the other is dust deposition (Jugder et al., 2011; Zhu et al., 2022). Determinations of physical weathering and dust deposition intensity may also help to improve the understanding of the amount of dust emissions occurring in the Gobi Desert. At present, it is still unclear how long the gravel layer on the Gobi Desert surface takes to be eroded to form a weathered layer of dust-sized fractions. Over the past thousand years, the gravel layer on the Gobi Desert surface has remained, suggesting that most dust deposition and dust-sized fractions produced by weathering are re-emitted, and the intensity of weathering and dust deposition may be the major components of dust emissions in the Gobi Desert. Physical weathering intensity here refers to the destructive effects of environmental factors on sand grains, gravel, or rocks during the physical weathering process. It can be quantified by the number of new cracks or daughter grains, the volume reduction of parent grains, or crack elongations per unit area during a finite period. Determination of the physical weathering intensity of the Gobi Desert may also help us to understand similar processes on asteroids. For example, previous studies (e.g., Hörz and Cintala, 1997) have estimated that basalt rock particles of 1 to 10 cm in diameter on the lunar surface will take millions of years to break up and form regolith, and that on the surface of some young asteroids consisting of centimeter-sized or smaller debris grains, the formation of regolith cannot be a result of meteoroid impact (Eppes et al., 2010). However, there are no field investigations on earth that would provide the observed data for supporting these speculations. Hence, more detailed case studies of physical weathering intensity under field conditions are still needed. Our previous study (Wang et al., 2020) indicated that the Gobi Desert is both a potential dust source area and a typical source-to-sink region, with deposition rate being greater than erosion rate. However, we did not report the physical weathering intensities of fractions having different particle sizes. Therefore, in this study, we report dust deposition and physical weathering intensity of materials of different particle sizes in the Gobi Desert from a more detailed experiment in order to evaluate the roles of these two processes in maintaining the Gobi Desert surface equilibrium.

2 Sampling and analysis methods

The experiment was conducted at the Guaizihu Meteorological Station (41.22°N, 102.22°E, 960 m a.s.l) located in the Ala Shan Gobi (one part of the Gobi Desert, Fig. 2). This region has mean annual precipitation of 45 mm, potential evaporation of 4201 mm, mean wind speed of 4.6 $m \cdot s^{-1}$, and mean annual air temperature of 9.3°C. The Gobi Desert landscape formed under the interactions of aeolian-fluvial processes, and can be derived from approximately 12 kyr BP (Hülle et al., 2010; Wang et al., 2020). Neotectonic processes and climate change during 1200–500 kyr BP may have impacted the evolution of the Gobi Desert (Wang et al., 2018; Lu et al., 2019). However, this region henceforth was under extremely arid climate and became an area of high dust emission in central Asia (Zhang et al., 2003; Wang et al., 2020). More details of the environment of this region were provided in Wang et al. (2005, 2012a, 2020).

Samples from the top 0–2 cm of the soil surface were collected at a specified location around the Guaizihu Meteorological Station. The sampling location was designed to be representative of the extensive geomorphic and landscape features of the Ala Shan Gobi, and can represent the general mechanism and process of physical weathering of the region. Each of the samples was sieved into size fraction groups of < 0.063, 0.063–0.125, 0.125–0.25, 0.25–0.5, 0.5–1, 1–2, 2–4, 4–8, 8–16, and > 16 mm. Each group except the < 0.063 mm was then washed with deionized water to remove the dust-sized fractions (< 0.063 mm in diameter) and air-dried. Five replicate samples (each about 300 g) from each group of 0.063–0.125, 0.125–0.25, 0.25–0.5, 0.5–1, and 1–2 mm, were placed into five sample pans with sieve pore size of 0.063 mm. For the fraction groups of 2–4, 4–8, 8–16, and > 16 mm, six replicate samples (five for the > 16 mm

Fig. 2 Spatial distribution of the Gobi Desert and the experimental site location (indicated by the red triangle in the figure). The locations of steppe, sandy desert, and Gobi Desert are from Kobayashi et al. (2017) and Yan and Wang (2019).

group) were placed into sample pans. The pan was covered by a screen with sieve pore size of 0.18 mm and was positioned on a bottom tray. The screen, pan, and tray all had the same diameter (20 cm), and were tightly bonded to constitute a self-designed device to simultaneously collect samples of physical weathering and dust deposition (Fig. 3). Devices for the fraction groups of 0.063–0.125, 0.125–0.25, 0.25–0.5, 0.5–1, and 1–2 mm were fixed in brackets at a height of approximately 2 m above the ground, and those devices for the groups of 2–4, 4–8, 8–16, and > 16 mm were anchored at a height of approximately 1 m above the ground beginning on 28 September 2020 (Fig. 3). These two heights were selected because at the 1-m and 2-m heights, it is usually very difficult for the coarse and fine (< 2 mm in diameter) fractions, respectively, of the near ground materials to be eroded and deposited in the sample pans. Approximately every 10 days, the dust-sized fractions within each device were sieved, collected and weighed using a balance with 0.0001 g precision. To determine the amount of physical weathering from the mixture amounts of dust deposition and physical weathering, five sample pans containing no raw samples were placed in brackets at a height of approximately 2 m above the ground to collect dust deposition at the same temporal intervals during the experimental period. Two HOBO temperature and humidity sensors (Onset Computer Corporation, Bourne, MA, USA) were individually placed in empty sample pans to monitor the temperature and relative humidity every 30 min.

The experiment lasted from 28 September 2020 to 18 December 2021. There was only 32 mm of precipitation during the period. To avoid the uncertainties caused by pretreatments, the dust-sized samples collected on 8

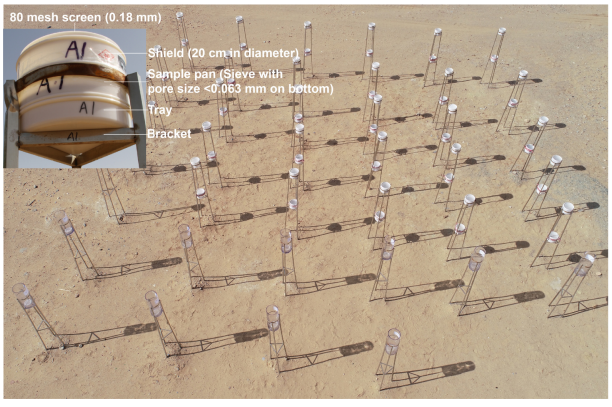

Fig. 3 Arrangement of experiment in the field. The inset (upper left corner) shows the structure of a sample pan. An 80 mesh screen was used to cover the sample pan because wind tunnel experiments had shown that with that cover, the sample within the pan would not be eroded under a wind velocity of 24 m/s.

October 2020 were not used for analysis. From 18 October 2020 to 18 December 2021, a total 41 runs of samples for each group were acquired, with two runs of outliers (collected on 28 November 2020 and 8 May 2021) being excluded. After the experiment was finished, samples in the pans were retrieved, weighed, washed with water through a < 0.063 mm sieve, air-dried, and weighed again. Particle size distributions of all samples were analyzed. For fraction groups of 0.063–0.125, 0.125–0.25, 0.25–0.5, 0.5–1, and 1–2 mm, a Mastersizer 3000 (Malvern Co. Ltd, Malvern, UK) was used to perform the particle size analysis. For fraction groups of 2–4, 4–8, 8–16, and > 16 mm, the particle size analysis was conducted by the sieving method.

The physical weathering intensity and dust deposition

of fraction groups of 0.063–0.125, 0.125–0.25, 0.25–0.5, 0.5–1, and 1–2 mm were the mean values of replicate samples ($g \cdot m^{-2}$), and the physical weathering intensity of fraction groups of 2–4, 4–8, 8–16, and > 16 mm was calculated as

$$PWI_c = \left(1 - \frac{\overline{X_s}}{\overline{X_{rc}}}\right) \times 100, \quad (1)$$

where PWI_c is the physical weathering intensity of each fraction group > 2 mm (%), $\overline{X_s}$ is the mean weight of the particles with the same and greater sizes than the raw samples of each fraction group after the experiment ($g \cdot m^{-2}$), and $\overline{X_{rc}}$ is the mean weight of raw samples of each fraction group ($g \cdot m^{-2}$).

Soluble salt contents and mineral analysis were conducted for six raw samples of each fraction group of < 0.063, 0.063–0.125, 0.125–0.25, 0.25–0.5, 0.5–1, and 1–2 mm. Salt contents were measured by the following steps. First, the samples > 0.1 mm were ground to ~0.1 mm in diameter with a rock mill, and 10 g of each ground samples was mixed with 50 mL of deionized water and oscillated for 10 min. The soil solution was then filtered through medium speed filter paper. Second, 10 mL of the filtered soil solution was placed in a wide-mouth crucible and steamed in a water bath. If the salt precipitate color was dark, a few drops of H_2O_2 were added to remove the organic matter. Third, the steamed samples were dried at 180°C for 24 h in an oven. Finally, the dried samples were weighed and salt contents were calculated. Detailed descriptions of the experimental processes are shown in Fig. 4. Samples of 2−5 g were ground into < 5 μm fractions, and an X'Pert Pro MPD powder X-ray diffractometer (XRD) (Rigaku Ultima IV, Japan) that scans with Cu *Kα* radiation at 3 kV was used for semiquantitative mineralogical analysis. The scan ranged from −110° to 180° with a precision of 0.002° and a resolution of 0.02°. After the scanning, the X-ray diffraction pattern of the sample was matched with various standard mineral patterns in the phase analysis software (Degen et al., 2014), and the mineral results (with relative errors of about 10%) were acquired.

Particle size, salt, and mineral analyses were done in the Oil and Gas Research Center, North-west Institute of Eco-Environment and Resources, Chinese Academy of Sciences, China. The temperature and relative humidity data were downloaded from the HOBO sensors after the experiment and are shown in Fig. 5.

3 Results

The amounts of dust-sized fractions produced by both physical weathering and dust deposition from 18 October 2020 to 18 December 2021 were 1387 ± 124, 702 ± 70, 698 ± 47, 742 ± 101, and 769 ± 75 $g \cdot m^{-2}$ for fraction groups of 0.063–0.125, 0.125–0.25, 0.25–0.5, 0.5–1, and 1–2 mm, respectively (Fig. 6). The highest dust-sized fraction appeared during 20 March and 1 April in 2021 when a heavy dust storm event occurred in the study area. Dust deposition during the same period amounted to 611 ± 55 $g \cdot m^{-2}$. For fraction groups of 0.063–0.125, 0.125–0.25, 0.25–0.5, 0.5–1, and 1–2 mm, there were 5.32 ± 0.76% (mean ± one standard deviation), 0.58 ± 0.27%, 0.53 ± 0.18%, 0.80 ± 0.52%, and 0.98 ± 0.31%, respectively, of the samples (by weight) having been weathered into dust-sized fractions. For the coarse fraction groups of 2–4, 4–8, 8–16, and > 16 mm, the particle sizes of the weathered materials were less than the particle sizes of the parent materials. Therefore, the method of washing the dust-sized fractions adhered to the parent materials and particle size analysis could accurately determine the physical weathering intensity of these coarse groups. During the approximately 14 calendar months (from 28

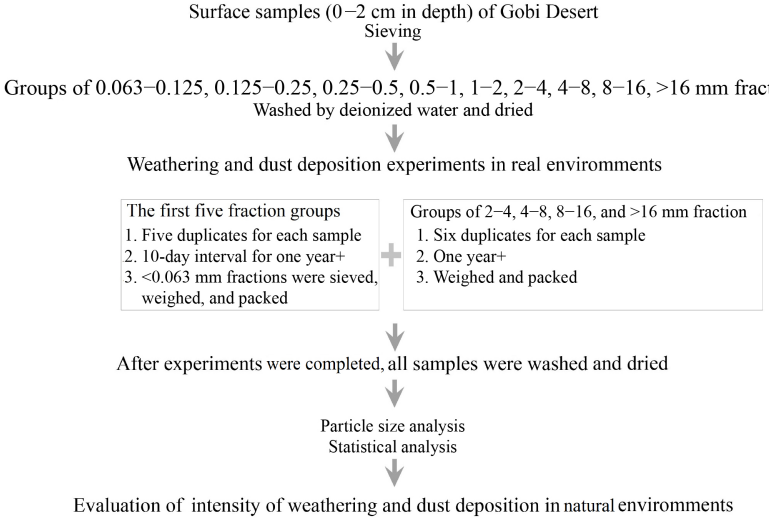

Fig. 4 Experiment flowchart.

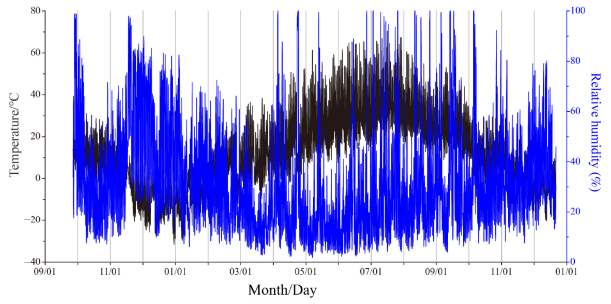

Fig. 5 Temperature and relative humidity recorded by HOBO sensors during the experimental period.

September 2020 to 18 December 2021) of the experiment, the physical weathering intensities for the fraction groups of 2–4, 4–8, 8–16, and > 16 mm were 23.95%, 14.96%, 8.90%, and 2.81%, respectively (Fig. 7).

4 Discussion

Previous studies have shown that gravel presently covers 18%–43% (average of about 30%) of the Gobi Desert surface (Wang et al., 2011, 2012b). Over the past thousands of years, the Gobi Desert has maintained a surface topographical equilibrium. This is due to the balance between dust-sized particles transported by the alluvial-diluvial processes and dust-sized particles produced by physical weathering and via dust deposition (Wang et al., 2020). The alluvial-diluvial processes have determined the characteristics of surface gravel in the Gobi Desert (Hülle et al., 2010). The clay layer within the Gobi Desert stratum was regarded as a product of alluvial processes that occurred in the Quaternary (Owen et al., 1997). Because of extremely low precipitation during the modern times, there have been essentially no extensive alluvial-diluvial processes occurring in the study region. On the other hand, decreased wind activity during the geological periods may have contributed to the deposition of dust-sized fractions on the Gobi Desert surface. After the gravel layer was developed on the Gobi Desert surface, the dust-sized fractions produced by physical, chemical, salt, and biological weathering processes (Wang et al., 2020) were eroded and transported. The Gobi Desert developed into a sandy desert or a desert with a clay layer covering the surface, becoming a dominant source area for Asian dust storms (Wang et al., 2017, 2019). Once the dust-sized fractions of the surface were eroded away, gravel in the underlying sediments was pushed upward (Springer, 1958; Inglis, 1965) and accumulated on the desert surface with variations in soil moisture and temperature. The processes of physical weathering, deposition, and erosion occurred in cycles day after day. Dust deposition in this study was 611 $g \cdot m^{-2}$, and the mean amount of dust-sized fractions produced by physical weathering was 249 $g \cdot m^{-2}$ from 18 October 2020 to 18 December 2021. Assuming that the density of Gobi Desert soil is 2.8×10^3 $kg \cdot m^{-3}$ (Shao et al., 2006), the thickness of dust-sized fractions produced via dust deposition and by physical weathering within the experimental period exceeded 0.31 mm. However, field investigations showed no evident changes in the Gobi Desert landscapes, indicating that most dust-sized fractions produced by physical weathering and via

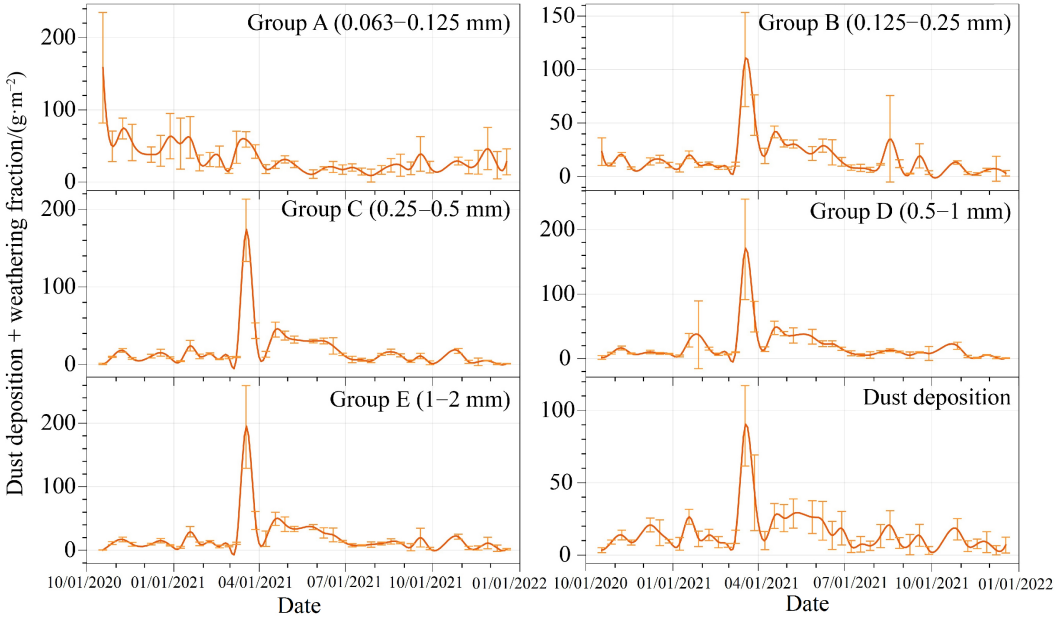

Fig. 6 Mean amounts of dust-sized fractions (< 0.063 mm in diameter) produced by physical weathering and by dust deposition. For each group (A to E) and for dust deposition, the number of replicate samples was five. The error bars in the figure indicate ± 1 standard deviation.

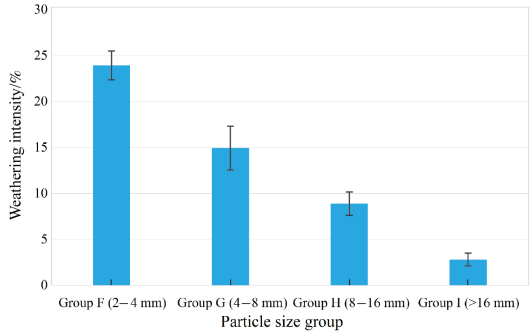

Fig. 7 Physical weathering intensity of fraction groups > 2 mm. For groups 2–4, 4–8, and 8–16 mm, six samples were used in the statistical analysis, and for the fraction group > 16 mm, five replicate samples were involved. The error bars in the figure indicate ± 1 standard deviation.

dust deposition were re-emitted during the experimental period.

Our previous study found no significant correlations between the temperature/moisture conditions and the intensity of physical weathering (Wang et al., 2020). The results of the current study showed that there were different correlations between the two climatic parameters and the amounts of dust-sized fractions produced by physical weathering and by dust deposition from different particle size groups (Table 1). We observed significant negative correlations between temperature and the dust-sized fractions from the 0.063–0.125 mm group, and between relative humidity and the dust-sized fractions from the groups of 0.125–0.25, 0.25–0.5, 0.5–1, and 1–2 mm. Due to the different combinations of hydrothermal climate conditions in the natural Gobi Desert environment, physical weathering intensity and mechanisms may vary among seasons. Freeze–thaw or cryogenic weathering occurring in winter may result in a large amount of weathering products, as has been observed in indoor and field experiments (e.g., Hall et al., 2005; Viles and Goudie, 2013; Lamp et al., 2017; Wang et al., 2020). For example, rapid low-temperature (< 0°C) variations between day and night in the winter season may lead to continuous expansion and contraction of rock minerals from inside to outside, accelerating rock fatigue (e.g., Lamp et al., 2017). Thermal fatigue can also set in at lower rates of temperature change, and is critical for rock breakdown in desert areas such as the Namib Desert (Viles and Goudie, 2013). Therefore, the negative correlations between temperature and the dust-sized fractions from the 0.063–0.125 mm group observed in this study may reflect the controls of physical weathering processes by the seasonal variations of climate. The negative correlations between the dust-sized fractions from the groups of 0.125–0.25, 0.25–0.5, 0.5–1, and 1–2 mm and relative humidity may further confirm the existence and effectiveness of low-temperature weathering. Under low temperature conditions (< 0°C) in winter on the Gobi Desert, the relative humidity decreased with decreasing temperature, and the retention of solid water (ice) in the environment increased. Frequent heating and cooling at diurnal cycles has been proven to play an important role in the generation of rock debris in extremely arid areas (Leask and Wilson, 2003). The particle fractions of the groups of 0.125–0.25, 0.25–0.5, 0.5–1, and 1–2 mm were coarser than those of the 0.063–0.125 mm group. The crushing efficiency may be increased with both increasing ice contents and an enhancement of freezing-thawing of ice at diurnal cycles.

Even though the sample pans were covered by an 80-mesh screen (0.18 mm in diameter) to prevent wind erosion, some fractions < 0.18 mm may still have been transported into the samples during the experiment. The particle sizes of the raw samples may thus be changed. However, variations in the main composition of each fraction group were still essential for determining the physical weathering intensity in the experiment. At the end of the experiment, for fraction groups of 0.25–0.5, 0.5–1, and 1–2 mm, the weight of samples in the pans decreased by 7.79%, 7.88%, and 13.01%, respectively (Fig. 8). These results indicated that the physical weathering intensities of these groups in field were not less than these values. In addition, mean physical weathering intensity of the > 2 mm fraction was 12.66% during approximately 14 calendar months. Therefore, the

Table 1 Correlations between temperature or relative humidity conditions and the dust-sized fractions produced by dust deposition and by physical weathering

Group	Temperature			Relative humidity		
	Pearson correlation	Significance (2-tailed)	*N*	Pearson correlation	Significance (2-tailed)	*N*
Group A (0.063–0.125 mm)	–0.404*	0.011	39	0.15	0.362	39
Group B (0.125–0.25 mm)	0.104	0.527	39	–0.443**	0.005	39
Group C (0.25–0.5 mm)	0.064	0.697	39	–0.409**	0.01	39
Group D (0.5–1 mm)	0.041	0.804	39	–0.428**	0.007	39
Group E (1–2 mm)	0.062	0.706	39	–0.396*	0.013	39
Dust deposition	0.041	0.806	39	–0.406*	0.01	39

Note: * Correlation is significant at the 0.05 level (2-tailed). ** Correlation is significant at the 0.01 level (2-tailed).

production of dust-sized particles via dust deposition and by physical weathering and re-emission of dust-sized particles under wind activities also played an important role in the Gobi Desert surface equilibrium.

Several factors affect the physical weathering intensity of Gobi Desert materials in natural environments. First, salts have an important impact on physical weathering (e.g., Goudie et al., 2002; Viles and Goudie, 2007). Before conducting this experiment, all raw samples were washed to remove the dust-sized fractions and soluble salts attached on the surface of the particles. However, the intergranular/intercrystalline salts contained in the particles were not excluded. These salts could have been released or reabsorbed on the surface of the particles as particles were broken or crushed. For instance, the mean soluble salt contents for raw samples of the 0.063–0.125, 0.125–0.25, 0.25–0.5, 0.5–1, and 1–2 mm groups (n = 6) were 0.83 ± 0.29, 0.56 ± 0.10, 0.96 ± 0.25, 0.57 ± 0.07, and 0.55 ± 0.10 g·kg^{-1}, respectively. In addition, the salt content of dust deposition was 1.99 ± 0.37 g·kg^{-1} (n = 6). During the experiment, salts were deposited into the raw samples, and consequently increased the physical weathering intensity of the raw samples. Second, the particle sizes of materials are also key factors controlling physical weathering intensity. Although we cannot accurately determine the physical weathering intensity of the 0.063–2 mm fraction groups, the physical weathering intensity of the > 2 mm groups decreased with increasing particle sizes of raw samples (Fig. 7). This result indicated that the gravel materials with small particle sizes were more sensitive to physical weathering in the field. Third, differences in mineral composition also play an important role on physical weathering intensity (e.g., Nesbitt and Young, 1989; Hall et al., 2005; Viles and Goudie, 2013). Mineral analyses of the raw samples showed that the plagioclase contents for the fraction groups of 0.063–0.125, 0.125–0.25, 0.25–0.5, 0.5–1, 1–2, and > 2 mm were 19.1 ± 3.4%, 19.0 ± 3.9%, 25.0 ± 2.2%, 39.4 ± 2.7%, 37.9 ± 0.4%, and 31.8 ± 2.3%, respectively. The differences in the plagioclase contents may also cause variations in physical weathering intensity among different particle fractions as previous studies have suggested.

5 Conclusions

A field experiment was conducted in the Ala Shan Gobi from September 2020 to December 2021 to determine the effects of physical weathering and dust deposition on the production of dust-sized fractions from different particle fractions of the Gobi Desert surface. The results showed that over approximately 14 calendar months (from 18 October 2020 to 18 December 2021), the dust-sized

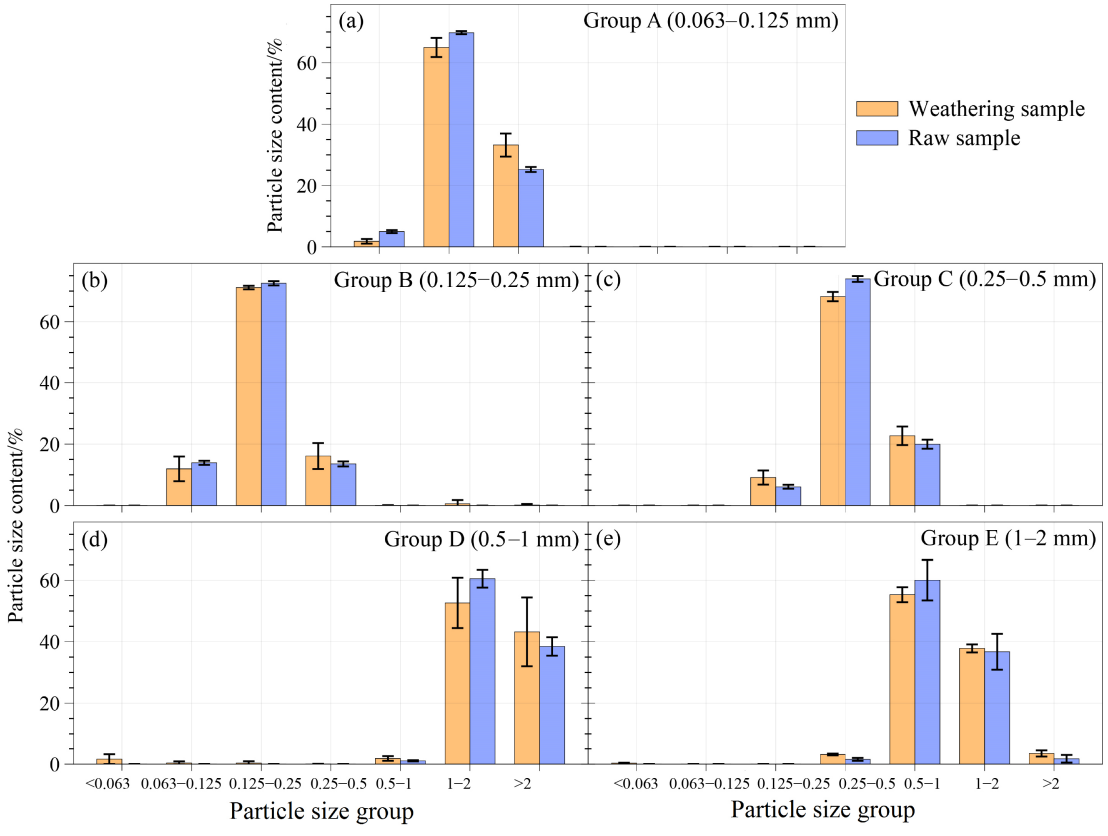

Fig. 8 Comparisons of the particle size distributions for experimental samples and raw samples. Five replicate samples were measured for each group. The error bars in the figure indicate ± 1 standard deviation.

fractions (< 0.063 mm in diameter) produced by physical weathering and via dust deposition in fraction groups of 0.063–0.125, 0.125–0.25, 0.25–0.5, 0.5–1, and 1–2 mm were 1387 ± 124, 702 ± 70, 698 ± 47, 742 ± 101, and 769 ± 75 $g \cdot m^{-2}$, respectively, and the dust deposition during the same period was 611 ± 55 $g \cdot m^{-2}$. In addition, for the fraction groups of 0.063–0.125, 0.125–0.25, 0.25–0.5, 0.5–1, and 1–2 mm, 5.32 ± 0.76%, 0.58 ± 0.27%, 0.53 ± 0.18%, 0.80 ± 0.52%, and 0.98 ± 0.31%, respectively, of the samples (by weight) were weathered into dust-sized fractions during the experimental period. Within approximately 14 calendar months (28 September 2020 to 18 December 2021), the physical weathering intensities for fraction groups of 2–4, 4–8, 8–16, and > 16 mm were 23.95%, 14.96%, 8.90%, and 2.81%, respectively. Relatively finer materials of the gravel were more sensitive to physical weathering than coarse materials. Physical weathering intensity in the Gobi Desert was far greater than those reported in previous studies. The amounts of dust-sized fractions produced by dust deposition and physical weathering and the Gobi Desert surface equilibrium indicated that the Gobi Desert was a key potential source area for Asian dust emissions. Dust deposition and physical weathering are both key factors affecting the Gobi Desert surface equilibrium in the natural environment of this study.

Acknowledgments This work was supported by the National Natural Science Foundation of China (Grant No. 41930640) and Key Frontier Program of Chinese Academy of Sciences (No. QYZDJ-SSWDQC043).

Competing interests The authors declare that they have no competing interests.

References

Ban G, Ban Z, Ma X (1962). 105 A.D. History of the Han Dynasty. Beijing: Chung Hwa Book.

Buckman S, Morris R H, Bourman R P (2021). Fire-induced rock spalling as a mechanism of weathering responsible for flared slope and inselberg development. Nat Commun, 12(1): 2150

Camuffo D (1995). Physical weathering of stones. Sci Total Environ, 167(1−3): 1–14

Cooke R U (1970). Stone pavement in deserts. Ann Assoc Am Geogr, 60(3): 560–577

Degen T, Sadki M, Bron E, König U, Nénert G (2014). The HighScore suite. Powder Diffr, 29(S2): S13–S18

Dorn R I (2011). Revisiting dirt cracking as a physical weathering process in warm deserts. Geomorphology, 135(1−2): 129–142

Eppes M C, McFadden L D, Wegmann K W, Scuderi L A (2010). Cracks in desert pavement rocks: further insights into mechanical weathering by directional insolation. Geomorphology, 123(1−2): 97–108

Filonchyk M (2022). Characteristics of the severe March 2021 Gobi Desert dust storm and its impact on air pollution in China. Chemosphere, 287: 132219

Goudie A S, Wright E, Viles H A (2002). The roles of salt (sodium nitrate) and fog in weathering: a laboratory simulation of conditions in the northern Atacama Desert, Chile. Catena, 48(4): 255–266

Hall K, Arocena J M, Boelhouwers J, Zhu L (2005). The influence of aspect on the biological weathering of granites: observations from the Kunlun Mountains, China. Geomorphology, 67(1−2): 171–188

Heumann M J, Johnson C L, Webb L E (2018). Plate interior polyphase fault systems and sedimentary basin evolution: a case study of the East Gobi Basin and East Gobi Fault Zone, southeastern Mongolia. J Asian Earth Sci, 151: 343–358

Hörz F, Cintala M J (1997). Impact experiments related to the evolution of planetary regoliths. Meteorit Planet Sci, 32(2): 179–209

Hülle D, Hilgers A, Radtke U, Stolz C, Hempelmann N, Grunert J, Felauer T, Lehmkuhl F (2010). OSL dating of sediments from the Gobi Desert, Southern Mongolia. Quat Geochronol, 5(2−3): 107–113

Inglis D R (1965). Particle sorting and stone migration by freezing and thawing. Science, 148(3677): 1616–1617

Jugder D, Shinoda M, Sugimoto N, Matsui I, Nishikawa M, Park S U, Chun Y S, Park M S (2011). Spatial and temporal variations of dust concentrations in the Gobi Desert of Mongolia. Global Planet Change, 78(1−2): 14–22

Kobayashi T, Tateishi R, Alsaaideh B, Sharma R C, Wakaizumi T, Miyamoto D, Bai X, Long B D, Gegentana G, Maitiniyazi A, Cahyana D, Haireti A, Morifuji Y, Abake G, Pratama R, Zhang N, Alifu Z, Shirahata T, Mi L, Iizuka K, Yusupujiang A, Rinawan F R, Bhattarai R, Phong D X (2017). Production of global land cover data-GLCNMO2013. J Geogr Geol, 9(3): 1–15

Lamp J L, Marchant D R, Mackay S L, Head J W (2017). Thermal stress weathering and the spalling of Antarctic rocks. J Geophys Res Earth Surf, 122(1): 3–24

Leask H J, Wilson L (2003). Heating and cooling of rocks on Mars: consequences for weathering. In: Lunar and Planetary Science Conference, 34: 1320

Lehmkuhl F, Nottebaum V, Hülle D (2018). Aspects of late Quaternary geomorphological development in the Khangai Mountains and the Gobi Altai Mountains (Mongolia). Geomorphology, 312: 24–39

Liu T, Ye L, Wang X, Pan Z (2007). Chemical action is an important factor for rock weathering in arid areas. Simulation experiments of evaporation and leaching. Geol China, 34: 815–821 (in Chinese)

Liu X, Wang H, Zuo H, Yan M, Li K (2022). Fractal of the Gobi surface sediment components and its variability characteristics. Catena, 218: 106525

Lu H, Wang X, Wang X, Chang X, Zhang H, Xu Z, Zhang W, Wei H, Zhang X, Yi S, Zhang W, Feng H, Wang Y, Wang Y, Han Z (2019). Formation and evolution of Gobi Desert in central and eastern Asia. Earth Sci Rev, 194: 251–263

McFadden L D, Eppes M C, Gillespie A R, Hallet B (2005). Physical weathering in arid landscapes due to diurnal variation in the direction of solar heating. Geol Soc Am Bull, 117(1): 161–173

Mu Y, Wang F, Zheng B, Guo W, Feng Y (2018). McGET: a rapid image-based method to determine the morphological characteristics

of gravels on the Gobi Desert surface. Geomorphology, 304: 89–98

Nesbitt H W, Young G M (1989). Formation and diagenesis of weathering profiles. J Geol, 97(2): 129–147

Ollier C D (1969). Weathering. Edinburgh: Oliver & Boyd, 304

Owen L A, Windley B F, Cunningham W D, Badamgarav J, Dorjnamjaa D (1997). Quaternary alluvial fans in the Gobi of southern Mongolia: evidence for neotectonics and climate change. J Quaternary Sci, 12(3): 239–252

Pelletier J D, Cline M, DeLong S B (2007). Desert pavement dynamics: numerical modeling and field-based calibration. Earth Surf Process Landf, 32(13): 1913–1927

Shao M, Wang Q, Huang M (2006). Soil Physics. Beijing: Higher Education Press, 320

Springer M E (1958). Desert pavement and vesicular layer of some desert soils in the desert of the Lahontan Basin. Soil Science Society of America, 22: 63–66

Vassallo R, Ritz J F, Braucher R, Carretier S (2005). Dating faulted alluvial fans with cosmogenic ^{10}Be in the Gurvan Bogd mountain range (Gobi-Altay, Mongolia): climatic and tectonic implications. Terra Nova, 17(3): 278–285

Viles H A, Goudie A S (2007). Rapid salt weathering in the coastal Namib desert: implications for landscape development. Geomorphology, 85(1−2): 49–62

Viles H A, Goudie A S (2013). Weathering in the central Namib Desert, Namibia: controls, processes and implications. J Arid Environ, 93: 20–29

Wang F, Li Z, Wang X, Li B, Chen F (2018). Variation and interplay of the Siberian High and westerlies in central-east Asia during the past 1200 kyr. Aeolian Res, 33: 62–81

Wang X, Cai D, Sun J, Lu H, Liu W, Qiang M, Cheng H, Che H, Hua T, Zhang C (2019). Contributions of modern Gobi Desert to the Badain Jaran Desert and the Chinese Loess Plateau. Sci Rep, 9(1): 985

Wang X, Cai D, Zhu B, Lou J, Li D, Zhang C, Chen S, Xu Y, Cai W, Su S, Che H (2020). Dust-sized fractions from dustfall and physical weathering in the Gobi Desert. Aeolian Res, 43: 100565

Wang X, Cheng H, Che H, Sun J, Lu H, Qiang M, Hua T, Zhu B, Li H, Ma W, Lang L, Jiao L, Li D (2017). Modern dust aerosol availability in northwestern China. Sci Rep, 7(1): 8741

Wang X, Dong Z, Yan P, Yang Z, Hu Z (2005). Surface sample collection and dust source analysis in northwestern China. Catena, 59(1): 35–53

Wang X, Dong Z, Zhang J, Liu L (2004). Modern dust storms in China: an overview. J Arid Environ, 58(4): 559–574

Wang X, Hua T, Zhang C, Lang L, Wang H (2012a). Aeolian salts in Gobi deserts of the western region of Inner Mongolia: gone with the dust aerosols. Atmos Res, 118: 1–9

Wang X, Lang L, Hua T, Wang H, Zhang C, Wang Z (2012b). Characteristics of the Gobi Desert and their significance for dust emissions in the Ala Shan Plateau (Central Asia): an experimental study. J Arid Environ, 81: 35–46

Wang X, Xia D, Wang T, Xue X, Li J (2008). Dust sources in arid and semiarid China and southern Mongolia: impacts of geomorphological setting and surface materials. Geomorphology, 97(3−4): 583–600

Wang X, Zhang C, Wang H, Qian G, Luo W, Lu J, Wang L (2011). The significance of Gobi Desert surfaces for dust emissions in China: an experimental study. Environ Earth Sci, 64(4): 1039–1050

Yan C, Wang J (2019). Dataset of Desert (Sandy Land) in China (1:100000). National Cryosphere Desert Data Center

Yu K, Lehmkuhl F, Schlütz F, Diekmann B, Mischke S, Grunert J, Murad W, Nottebaum V, Stauch G, Zeeden C (2019). Late Quaternary environments in the Gobi Desert of Mongolia: vegetation, hydrological, and palaeoclimate evolution. Palaeogeogr Palaeoclimatol Palaeoecol, 514: 77–91

Zhang X, Gong S, Zhao T, Arimoto R, Wang Y, Zhou Z (2003). Sources of Asian dust and role of climate change versus desertification in Asian dust emission. Geophys Res Lett, 30(24): 2272

Zhu B, Zhang J, Sun C (2022). Potential links of Gobi, dust, and desertification: a comprehensive understanding from aeolian landform evolution in a middle-latitude desert. Sediment Geol, 428: 106049

Zobeck T M (1991). Soil properties affecting wind erosion. J Soil Water Conserv, 46(2): 112–118